Heki and Jin *Satellite Navigation* (2023) 4:24
https://doi.org/10.1186/s43020-023-00113-6

Satellite Navigation
https://satellite-navigation.springeropen.com/

REVIEW

Open Access

Geodetic study on earth surface loading with GNSS and GRACE

Kosuke Heki[1,2*] and Shuanggen Jin[1,3]

Abstract

Ice, snow, and liquid water on the surface of the Earth exert downward force onto the solid earth and deform the lithosphere typically in seasonal timescale. Space techniques, such as Global Navigation Satellite System (GNSS), made it possible to directly measure subtle displacements caused by loading. We can also observe such loads with time-variable gravity using gravity recovery and climate experiment satellites. These techniques made surface loads an attracting scientific target of modern geodesy. In this paper we briefly review the history of geophysical studies of surface loads through geodetic observations of crustal deformation and time-variable gravity. We also review advanced topics such as short-term crustal deformation due to severe meteorological episodes and monitoring of terrestrial water storages. We also present a few related topics such as the change of the obliquity of the Earth due to loads and artificial crustal subsidence signals caused by snow accretion onto GNSS antenna radomes.

Keywords GNSS, GRACE, Seasonal change, Surface load, Land hydrology, Snow

Introduction: what is load for geodesists?

Atmosphere and water on the Earth's surface are highly mobile. Their large-scale redistribution causes a variety of geophysical phenomena and attracts the attention of geodesists in various disciplines of modern geodesy, i.e., positioning, gravity, and Earth rotation. Before the advent of space positioning techniques the large-scale redistributions of surface loads had been studied through the Earth's rotation. Mass movements changing the Earth's degree-2 tesseral components excite the polar motion, and those changing the Earth's moment of inertia about the present rotation axis change the length-of-day. Hence, observing the changes of the earth rotation parameters plays a major role in studying large-scale mass redistributions (e.g., Lambeck, 2005; Munk & Macdonald, 1960).

A load exerts a downward force (loading) and deforms the Earth's lithosphere. Vertical and radial displacements in a realistic layered spherical Earth as a response to a point load can be calculated using load Green's functions (e.g., Farrell, 1972). Figure 1 shows an example of the surface displacements caused by a load of one-meter depth water covering 2 × 2 degrees on the Earth (1 degree corresponds to ~ 110 km). This load, amounting to ~ 48 Gt in mass, causes only up to ~ 1 cm of subsidence. The geodesists working on crustal deformation are not much interested in such a load since the displacements are not large enough to be detected by the conventional non-global measuring techniques. In 1980s, international space geodetic campaigns of Very-Long-Baseline-Interferometry (VLBI) and Satellite-Laser-Ranging (SLR) started to measure the current motions of tectonic plates as well as the changes in Earth rotation parameters. Such global space geodetic techniques can detect the subtle deformations caused by surface loading.

Corrections of the displacements by ocean tidal loading together with solid earth tidal deformation have been

*Correspondence:
Kosuke Heki
heki@sci.hokudai.ac.jp
[1] Shanghai Astronomical Observatory, Chinese Academy of Science, Shanghai 200030, China
[2] Hokkaido University, N10 W8, Kita-ku, Sapporo, Hokkaido 060-0810, Japan
[3] School of Surveying and Land Information Engineering, Henan Polytechnic University, Jiaozuo 454000, China

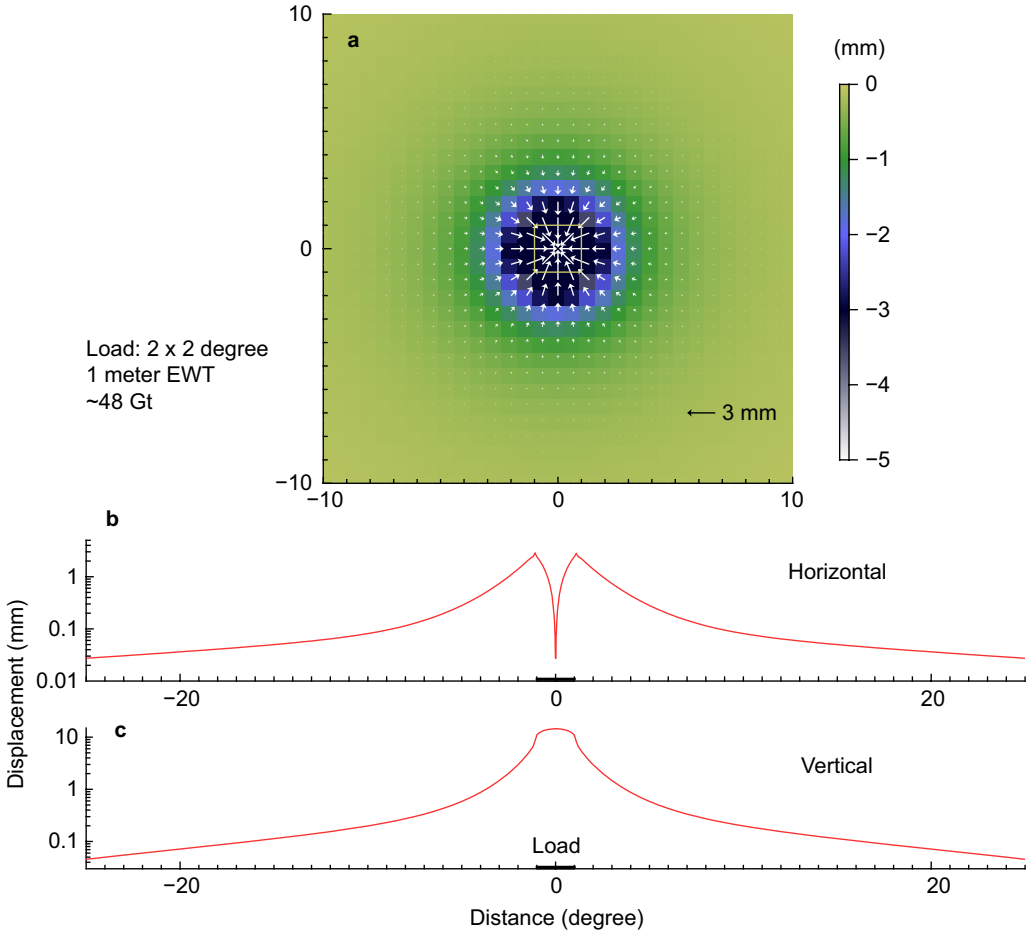

Fig. 1 Displacements caused by a load on the Earth with the dimension 2×2 degrees (yellow square) and with the equivalent water thickness of 1 m (**a**). East–west profile of the horizontal (**b**) and vertical (**c**) crustal movements caused by the loading. We used the Green's function given in Farrell (1972)

implemented in software packages analyzing the global space geodetic data from the beginning of international VLBI and SLR campaigns. As the measurement accuracy of space geodetic techniques improves, the uncorrected crustal deformations caused by atmospheric load changes were considered as a possible source of systematic errors in the baseline length time series, and van Dam and Wahr (1987) discussed the way to reduce the scatters of data by correcting for the displacements due to atmospheric loads on land. Nevertheless, international space geodetic campaigns are not frequently conducted and the stations are not densely deployed. In such a situation, surface loads were considered as a nuisance disturbing station position time series, rather than a scientific target.

In 1990s, Global Navigation Satellite System (GNSS) has come into use as the number of GPS (Global Positioning System) satellites increases. With a dense network of continuous receiving stations in a region of high tectonic activity it is possible to observe daily crustal movements with millimeter accuracy and high spatial resolution. Geodesists soon realized significant seasonal displacement signatures were overprinted to the secular movements of tectonic origin and started geophysical investigation of surface loading.

In Japan, Murakami and Miyazaki (2001) found a positive correlation between the seasonal movement amplitudes and interseismic movement speeds of Japanese stations. They interpreted it as a consequence of the seasonal changes of plate velocity, though this correlation was an artifact that emerged by fixing a station in the Japan Sea coast. Heki (2001) found east–west crustal shortening and extension occur in winter in the western and eastern side of the Northeast (NE) Japan backbone range, respectively, and hypothesized that they were caused by snow load accumulating on the western side of the range.

Dong et al. (2002) studied the various factors for such seasonal variations at GNSS stations worldwide and concluded that ~ 40% of such variations came from real crustal movements due to loading and pole tides. Heki (2004) performed a comprehensive study on the seasonal mass change in Japan, including snowpack, atmosphere, nontidal ocean loading, impoundment of reservoirs, and soil moisture, and concluded the snow load was a dominating factor in NE Japan. The seasonal crustal movements due to various surface loads are studied in many parts of the world, including Iceland (Drouin et al., 2016).

Figure 1 shows that a load brings only subsidence. On the other hand, horizontal displacements cause both extension and shortening, i.e., they occur in the outside and beneath the load, respectively. The key reason why Heki (2001) attributed the seasonal crustal deformation in NE Japan to snow loading was that the spacing among GNSS stations is smaller on the snow-covered western side of the backbone range while it becomes larger on the other snow-free side.

It is important to note that the subsidence is the largest at the center of the load (Fig. 1c) while the largest horizontal displacement occurs at the edge of the load (Fig. 1b). This is because horizontal movements reflect azimuthal asymmetry of load rather than the load at that point. Because the load is symmetrically distributed around the center of the load, the horizontal displacement does not emerge in spite of maximum subsidence. This difference causes different spatial distribution of horizontal and vertical displacements. This makes the spatial functions of the horizontal and vertical components for a given load different. It needs to be kept in mind in doing any analysis (e.g., principal component analysis) using three-dimensional (3D) displacement field.

After the launch of GRACE (Gravity recovery and climate experiment) satellites in 2002, it became possible to observe mass anomalies directly from space. Now we can see large-scale surface loads in two independent ways, surface displacements and mass anomalies. The early studies of GRACE versus GNSS (e.g., Bevis et al., 2005; Davis et al., 2004) showed that the two data sets can be directly compared by using the Stokes' coefficients of time-variable gravity from GRACE and the load Love numbers. This significantly made this field of studies more convincing.

For small-scale surface loads, however, satellite gravimetry is not as useful as GNSS receivers deployed densely around the loads. In such cases, it becomes important to compare the displacements measured with GNSS and those with independent sources such as meteorological data (e.g., precipitation, snow depth) and hydrological models. Studying small-scale loads may require additional factors, e.g., deviation of local elastic properties from the global average and viscoelasticity (Tang et al., 2020).

A popular topic is the link of time-variable loads to seasonal changes of earthquake occurrences. This has been discussed in the regions including Japan (Heki, 2003), Nepal (Bollinger et al., 2007), California (Johnson et al., 2017), and Taiwan (Hsu et al., 2021). Surface loading enhances the stress normal to the fault planes and discourage faulting. In other words, the removal of such loads encourages earthquakes. This is an important application of surface load study for geophysics, but we will not detail this issue in this article.

Seasonal crustal movements by surface loading

Land hydrological loads

We first show the seasonal displacements in the northern half of South America, where large land hydrological water load seasonally changes in a continental scale. In the tropical regions close to the equator, rainy and dry seasons alternate, resulting in positive and negative mass anomalies in these seasons. GRACE data, available from UTCSR as mascon solution (Save, 2019), are shown in Fig. 2. It shows that the change of ± 1 m in equivalent water thickness occurs every year. This amplitude is similar to the example given in Fig. 1.

Figure 2b shows the subsidence and uplift in the regions of positive and negative mass anomalies, respectively. On the other hand, horizontal movements reflect spatial gradient of mass anomalies, i.e., stations move in the direction from negative to positive mass anomalies. In both components, the amounts are not simply proportional to the local mass anomalies and their spatial gradients. In fact, close to a point load, the displacements are proportional to the inverse of the distance (Farrell, 1972) and reflect the integrated effects of surrounding mass anomalies. In the case of surface loads composed of complicated distributions of smaller scale anomalies, the displacements obtained from GNSS and the mass anomaly distribution got from GRACE are not so consistent with each other as in Fig. 2 ,i.e., they often show inconsistency due to the difference of spatial resolution of the two techniques (Zhang et al., 2021).

The time series (Fig. 2d) of Manaus, located at the center of the Amazon Basin, show peak-to-peak horizontal and vertical movements of up to 2 cm and 6 cm, respectively. This is one of the stations exhibiting the largest seasonal crustal movements in the world. We notice that the data often deviate from the average seasonal change curve. Such an interannual variability often reflects climate variability, such as smaller and larger amount of rain in austral summers in this region during the El Niño and La Niña episodes, respectively (Morishita

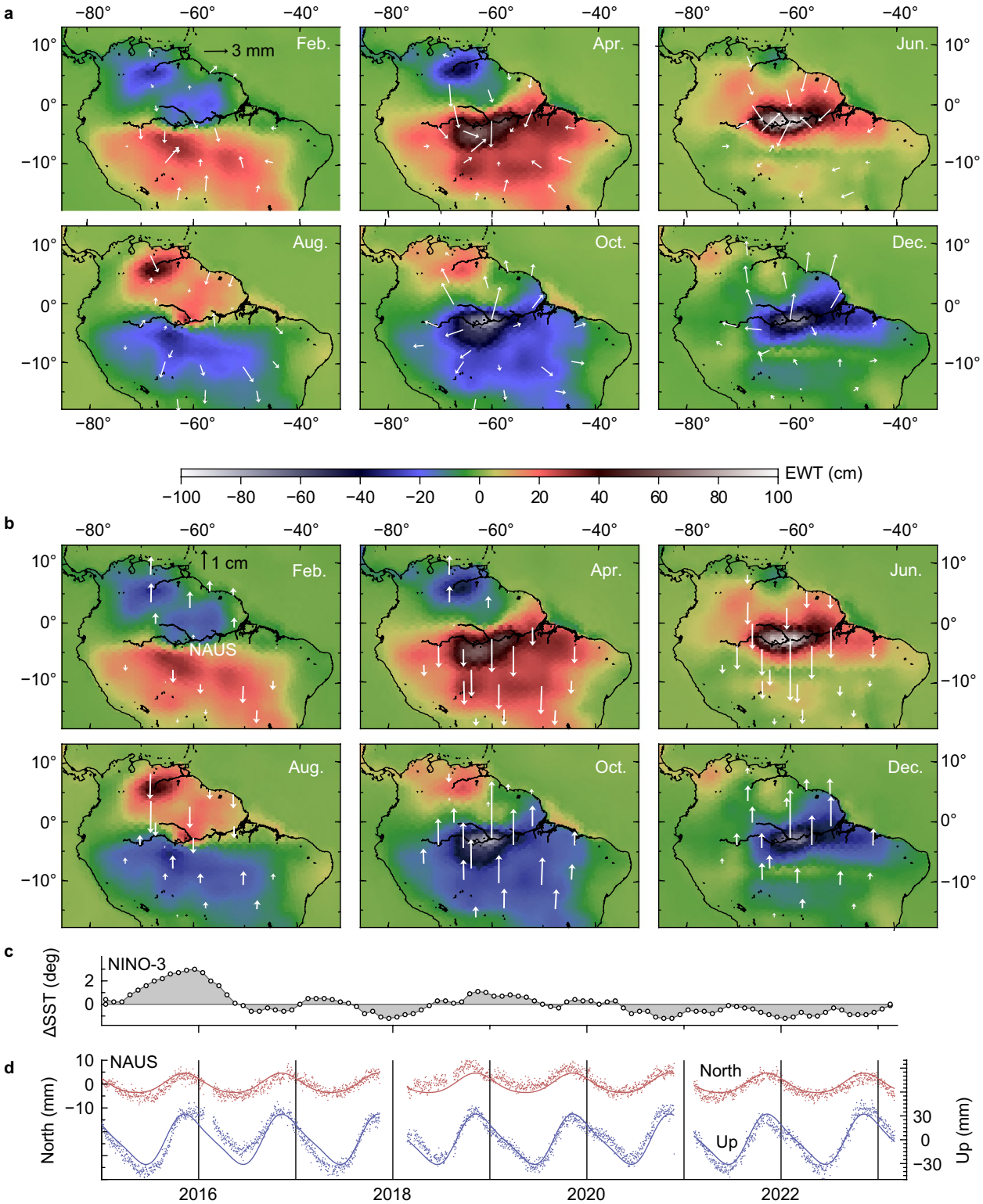

Fig. 2 Average horizontal (**a**) and vertical (**b**) displacements in 6 months at GNSS stations in northern South America. The data are from Nevada Geodetic Laboratory (NGL), Univ. Nevada Reno (UNR) (Blewitt et al., 2018), plotted with average seasonal mass anomaly distributions from CSR GRACE mascons (Save, 2019). The horizontal displacements reflect the direction of spatial mass gradient and the subsidence and uplift reflect the positive and negative mass anomalies, respectively. **d** The de-trended time series of north (red) and up (blue) components of NAUS (Manaus in the middle of the Amazon Basin) station are shown together with average seasonal (annual and semiannual) change curves. During an ENSO episode in 2015–2016 (**c**), abnormally small rain made NAUS uplift more than other years (**d**)

& Heki, 2008). Interannual changes will be also discussed in the next section.

Snow loads and interannual variations

The seasonal movements of GNSS stations do not repeat in the same pattern every year. They usually show interannual variations in amplitudes and phases. As shown in the previous section, the precipitation in the Amazon Basin is modulated interannually by El Niño-Southern Oscillation (ENSO) index, i.e., rainfall gets smaller when the ENSO index stays high (e.g., Ropelewski and Halpert, 1996). This can be confirmed in Fig. 2c, d, where the station position is shifted upward due to less water load during the 2016–2017 El Niño episode. The snow in high-latitude regions in the northern hemisphere are much influenced by the Arctic Oscillation (AO), and both time-variable gravity and seasonal crustal movement amplitudes show a high correlation with the AO indices (Matsuo & Heki, 2012).

Figure 3 shows an example of the seasonal crustal deformations by winter snows in Hokkaido Island, northern Japan, derived from the dense GNSS network in Japan, GEONET (GNSS Earth Observation Network). There the snow reaches a few meters deep in winter and causes strong seasonal crustal movement signatures. The two time series represent the crustal deformations due to snow loading, i.e., horizontal movement toward N135E (southeast) at a station in northwestern coast and vertical down component at a station within the snowiest region. We used the F5 solution of GEONET station positions by Geospatial Authority of Japan (GSI) (Takamatsu et al., 2023) and fixed a station (0015) in the southeast part of the island where the snow depth is insignificant.

The snow depths have large interannual variations, e.g., the snow on February 14 2020 is only about a half of the

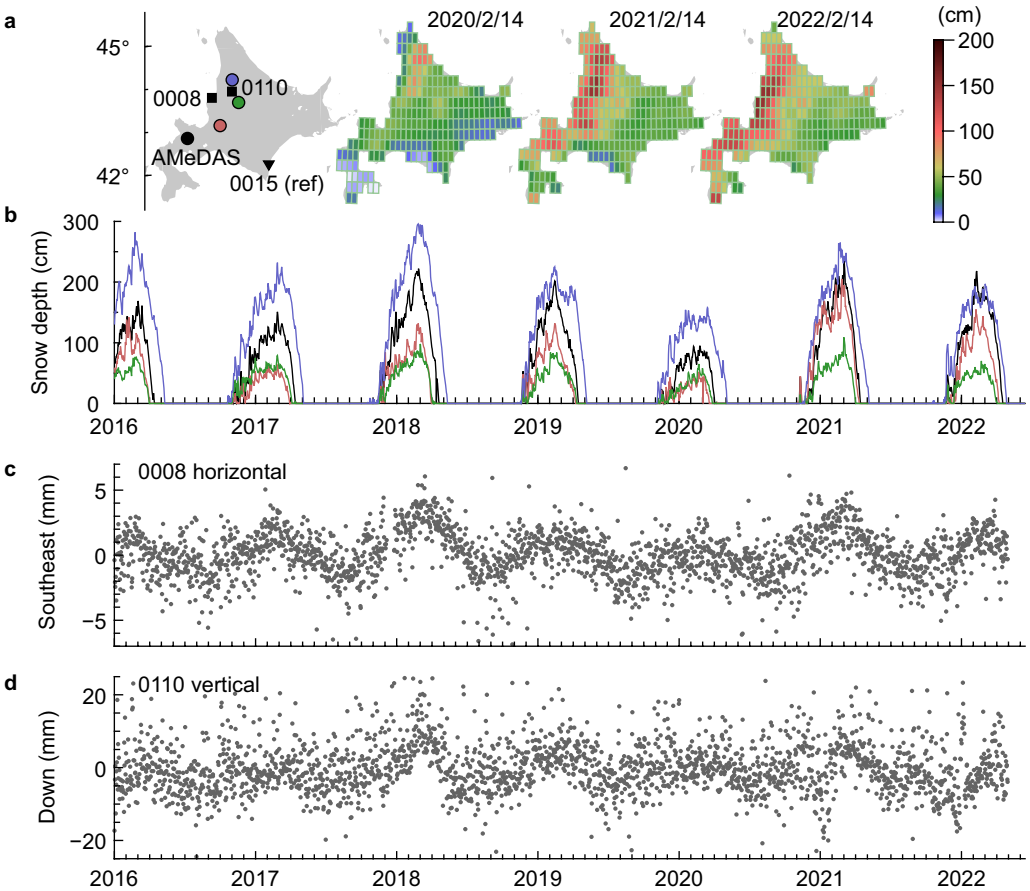

Fig. 3 Seasonal crustal movements by snow loading in Hokkaido, northern Japan. The snow depths are less in 2020 than in 2021/2022 (**a**). This is confirmed also in time series in (**b**) showing snow depth curves at four AMeDAS (Automatic meteorological data acquisition system) snow depth meters (position shown in the same color in the map). **c** indicates the horizontal displacement of a northwestern coastal station (0008) toward southeast (N135E) relative to a reference station in southeast (0015). **d** indicates the time series of down component at a station within a deep snow area (0110). **c** and **d** exhibit similar behavior, i.e., the peaks are strong in winters 2020–2021 and 2021–2022, and weaker in 2019–2020

snow on the same day in 2021 and 2022 (Fig. 3a, b). Such interannual differences are reflected in the crustal movements time series in horizontal and vertical directions in Fig. 3. Although the vertical movements of the station under the snowpack have larger amplitude (Fig. 3d), the signal-to-noise ratio seems better in the horizontal component of the coastal station (Fig. 3c). Another important point is that snow depths remain zero after April or May while station coordinate time series are not 'flat' even after that. This may be because the snow depth meters are deployed in valleys while snow remains in uninhabited mountains and melt only slowly during summer times.

Interference of ocean loading and land hydrological loading

Compared with land hydrological mass changes, oceans show much less variability in water mass because of high mobility of water in open oceans. However, semi-closed oceans may show large seasonal variations in mass driven by various seasonal factors. Red Sea is an example, which is located between North Africa and the Arabian Peninsula. Wahr et al. (2014) found seasonal mass changes with peak-to-peak amplitude amounting to ~ 50 cm in equivalent water depth in Red Sea using GRACE gravity data. These changes occur by heat exchange with atmosphere and flow through the strait to the Indian Ocean. Later, Alothman et al. (2020) reported seasonal horizontal and vertical crustal movements at GNSS stations on the Red Sea coast mainly driven by these ocean mass changes.

The data interpretation in the Red Sea case was straightforward because the sea is surrounded by the arid land and the ocean mass changes govern seasonal crustal movements there. A large seasonal mass change, with ~ 40 cm peak-to-peak amplitude, occurs in the Gulf of Carpentaria in northern Australian coast. This is driven by seasonal wind blowing into the gulf during the austral summer months. Unlike the Red Sea, this area is surrounded by tropical rain forest, and crustal movements at GNSS stations on its coast are rather complicated. Zheng et al. (2023) analyzed the seasonal changes in gravity and GNSS station positions and found that their phase and amplitudes can be interpreted by the interference of ocean and land seasonal mass changes with a significant phase lag.

Figure 4 illustrates the interference of two adjacent loads with the same amplitudes of seasonal mass changes. If they change in phase (Case 1), a coastal GNSS station shows strong seasonal vertical movements, but no horizontal movements. If they are opposite in phase

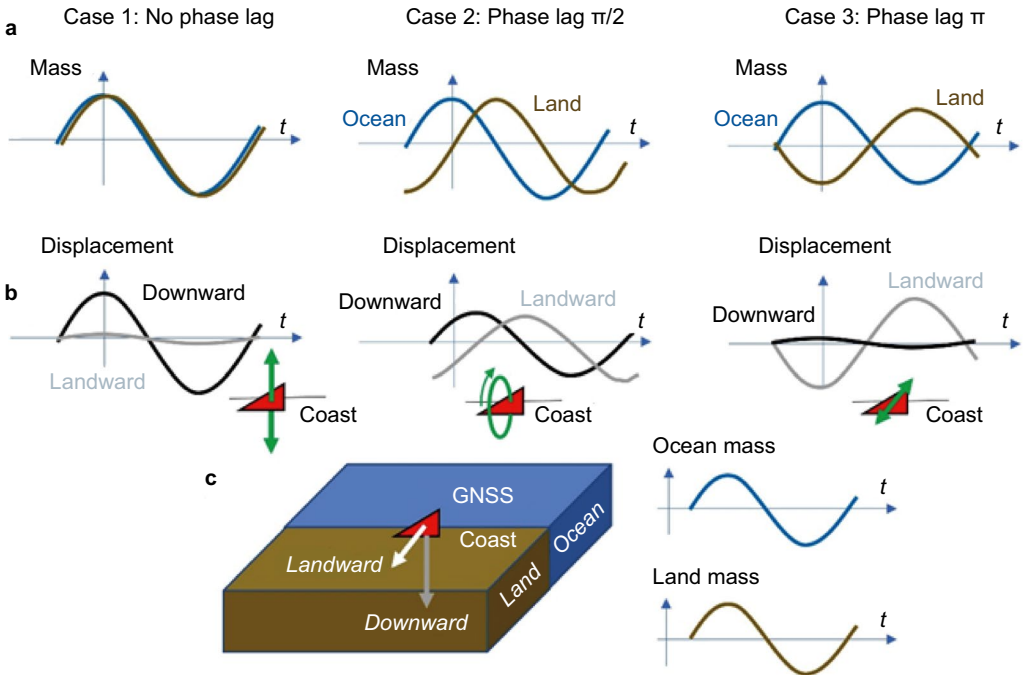

Fig. 4 Concept of interference of seasonal land and ocean mass changes (**c**) of comparable amplitudes but with phase lags (**a**). Horizontal (landward) movement reflects the difference between the land and the ocean masses, while vertical movement reflects the sum of both (**b**). In case 1 (left), 2 (middle), and 3 (right), the two masses change in phase, with phase lags of 90 and 180 degrees, respectively. In these cases, coastal GNSS stations show only vertical (Case 1) and horizontal (Case 3) displacements (green arrows). In Case 2, both horizontal and vertical seasonal crustal movement occur with different phases, and station movement trajectory becomes an ellipse. This occurs in the Gulf of Carpentaria in northern Australia (Zheng et al., 2023)

(Case 3), vertical movements are suppressed and only landward and oceanward horizontal seasonal movements prevail. In Case 2, ocean and land seasonal mass changes have a certain phase lag. In this case, both horizontal and vertical seasonal crustal movements occur, and they have different phases (station trajectory becomes an ellipse). The Gulf of Carpentaria is similar to Case 2, i.e., both ocean and land mass changes are significant in amplitude (change in the ocean is somewhat stronger), and the land mass changes lags behind the ocean mass by ~ 2 months. There, the peak vertical and horizontal displacement months shift from the ocean mass peak month in opposite senses (Zheng et al., 2023).

Similar complicated interference of crustal deformation caused by seasonal mass changes in the ocean and the land also occur in the Gulf of Thailand. The significant seasonal mass changes are clear in the GRACE time-variable gravity data. However, there are few appropriate continuous GNSS stations with sufficient data length along its coast, and interference of land and ocean seasonal mass changes have not been studied with GNSS data yet. Regarding large open oceans in general, seasonal mass changes are insignificant there. Hence, seasonal movements of coastal GNSS stations are governed by hydrological mass changes on land, i.e., they move landward during rainy seasons (Zheng et al., 2023).

Intra-seasonal crustal movements: heavy rain episodes

In the previous section, we reviewed the crustal deformations in seasonal timescales driven by the changes in surface loading. There are now increasing number of studies on the crustal deformations caused by surface loading in intra-seasonal timescales, e.g., days and weeks. They occur, for example, by heavy rain episodes brought by landfalls of tropical cyclones or activities of meteorological stationary fronts. Milliner et al. (2018) studied the crustal deformations in southern North America in response to stormwater loading of the Hurricane Harvey, which hit the coastal region of the Gulf of Mexico in 2017. Zhan et al. (2021), using GEONET in Japan, studied both the water vapor concentration and ground subsidence associated with the landfall of the super typhoon Hagibis, which drenched NE Japan in October 2019.

Both Milliner et al. (2018) and Zhan et al. (2021) used only vertical components because horizontal displacements, caused by azimuthal asymmetry of loads, are strongly influenced by small scale water distributions and difficult to interpret with the given GNSS station density. Short-term subsidence signatures are only up to 1–2 cm, and more attention is needed to the common mode errors in identifying those signals. In these two studies, the common mode errors were reduced to isolate subsidence signatures in daily timescales out of noisy vertical position time series. Zhan et al. (2021) compared the vertical position time series before and after correcting the common mode errors.

These two studies highlighted the different situations of terrain in estimating spatial distributions of water loads. Milliner et al. (2018) studied stormwater on a flat continental terrain in southern North America and successfully estimated water distribution using the crustal subsidence data as the input and the load Green's function as the model. On the other hand, Zhan et al. (2021) showed that such an inversion resulted in an overestimation of water loads. In mountainous island arcs like the Japanese Islands, rainwater rapidly gathers along valleys. Such a load concentration causes the excessive subsidence of GNSS stations that are selectively deployed along valleys.

Later, Heki and Arief (2022) studied the crustal subsidence caused by floods that hit Southwest (SW) Japan every summer 2017–2020. Heavy rains were caused by large amount of water vapor transported from the East China Sea along the stationary front extending east–west. They found a clear linear relationship between the total amount of daily rains and crustal subsidence on that day integrated over the whole SW Japan, and this linearity holds up to the rain intensity of ~ 10 Gt/day. This shows a clear contrast in the behavior from snowpack. Rainwater rapidly drains to the sea and is largely lost within a day in mountainous islands like Japan. Thus, it depresses the ground only during the day of precipitation. Snow, on the other hand, stays on land often for months until the spring thaw.

Here one may ask if it is possible to correct for subsidence due to rainwater loading by monitoring daily precipitation near GNSS stations. Figure 5 answers this question using the data in the heavy rain episode in August 2021 in SW Japan, a new episode not covered in Heki and Arief (2022). Figure 5 compares daily/hourly precipitation averaged over areas of various spatial scales, city/town level (a few tens of kilometers), prefecture level (~ 100 km), district level (a few hundreds of kilometers), and the whole SW Japan. We confirm the strong correlation between spatially averaged daily precipitation and subsidence over the whole SW Japan (Fig. 5, bottom). However, the correlation becomes low as we reduce the averaging area. This would reflect two factors. The first is the high mobility of water. It flows down rivers and causes downstream areas subside rather than the rain areas. The second factor is the decrease of random errors by averaging more measurements. Whichever factor is dominant, Fig. 5 suggests that it is impractical to correct

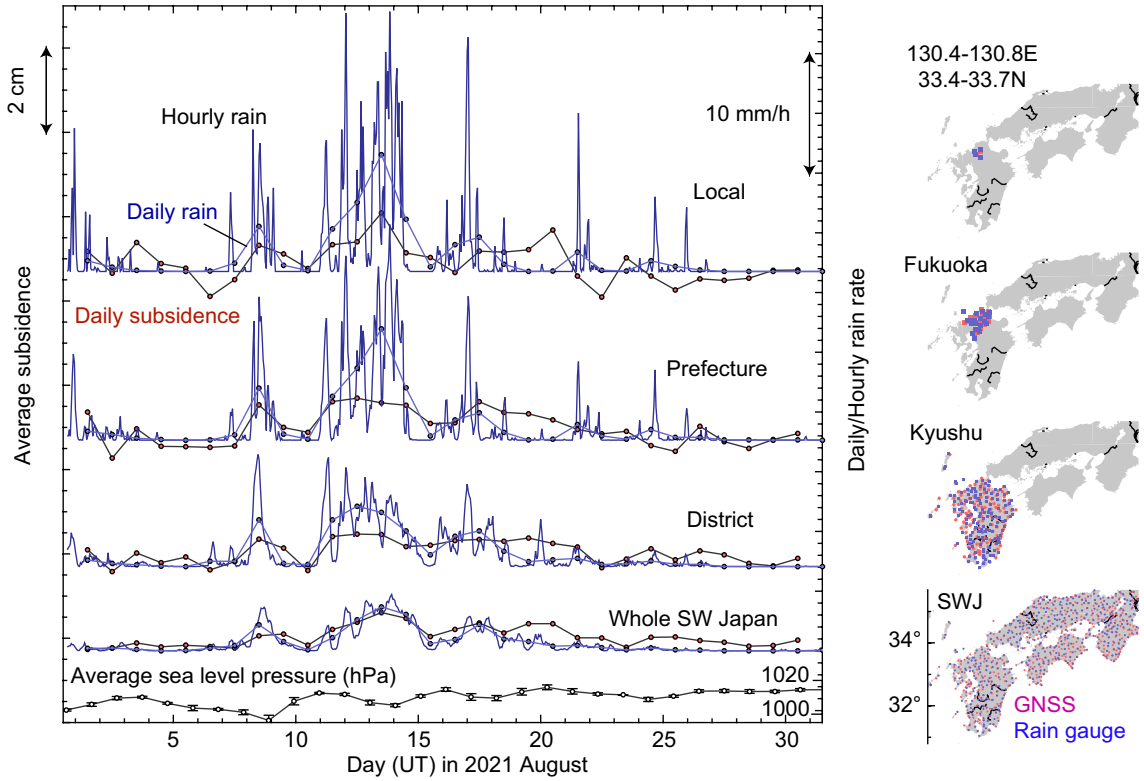

Fig. 5 Comparison of hourly (blue) and daily (blue, with dots) rain rates (both in mm/h), and average daily subsidence of GNSS stations (red) during August 2021 in Southwest Japan. AMeDAS rain gauge stations and GNSS stations are shown with blue and red dots in the map. Four data sets represent different averaging spatial scales, from top to bottom, a local scale, the Fukuoka Prefecture, the Kyushu Island (made of 7 prefectures), and the whole SW Japan. The correlation between rain and subsidence improves as we average over larger areas (0.61, 0.68, 0.73, 0.82 from top to bottom). Average sea level pressure data with 1σ error bars (bottom) are obtained from 30 barometers in SW Japan

for daily subsidence of a certain GNSS station using the data of a nearby rain gauge.

Steady subsidence of ~ 5 mm after the heavy rain episode is seen over the second half of August for the whole SW Japan. It is due to the increase of atmospheric pressure of ~ 10 hPa (equivalent to ~ 10 cm water depth) as a part of regular seasonal changes (Fig. 5 bottom).

Water storage variations and displacements of GNSS points

Seasonal water storage changes and vertical displacement amplitudes

The mass loading variations cause the deformation of the underlying Earth, which can be precisely measured by continuous GNSS observations, particularly in vertical direction. Therefore, the GNSS coordinate time series can be used to estimate the changes in mass loading, e.g., Total Water Storage (TWS) variations after removing ocean tide and atmospheric loading effects (Argus et al., 2014; Jin et al., 2022). The elastic displacement $u(\theta)$ can be expressed by the integration of the mass loading and Green's function (Wang et al., 2012; Zhang et al., 2017) as follows:

$$u(\theta) = \frac{\Delta M \times R}{M_e} \sum_{n=0}^{\infty} h_n P_n(\cos\theta) \quad (1)$$

where θ is the angular distance, R and M_e are the mean radius and mass of the Earth, respectively, ΔM is the mass load, h_n is the elastic Love number, and P_n are the Legendre polynomials. The load Love number is truncated up to degree 500 and the higher degree is ignored due to their little contribution to the displacement. The unknown mass load is discretized into grid cells with spatial resolutions of 0.5°–1° based on GNSS network density and the mass load at grid cells can be recovered (or inferred) from GNSS displacements.

A case study with the displacement data at 251 continuous GNSS stations in southwestern US was carried out to inverse water storage change. Figure 6 shows the

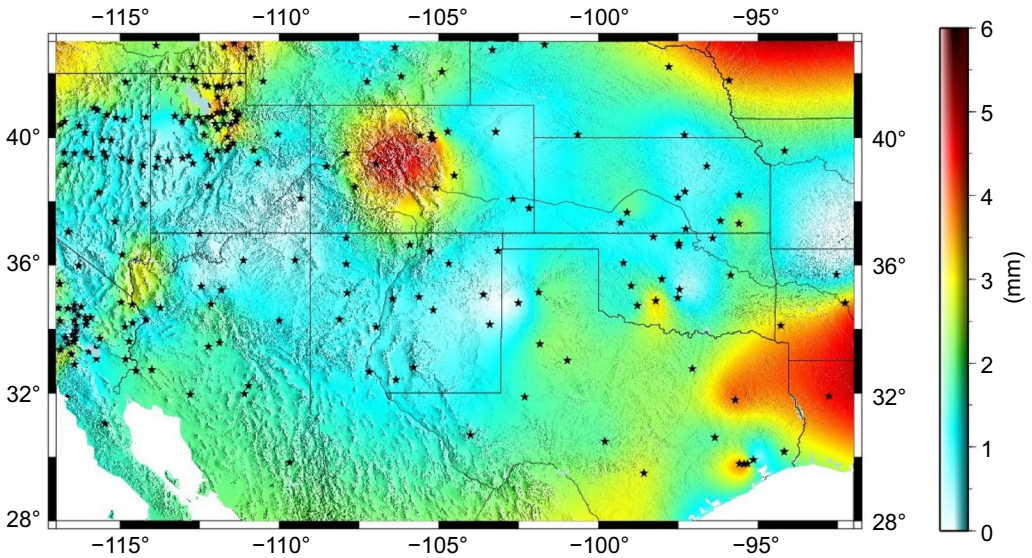

Fig. 6 The annual amplitude distribution of vertical displacements of GNSS stations in SW US (28°N–43°N, 92°W–117°W) (modified from Jin & Zhang, 2016)

distribution of the annual amplitude of vertical GNSS station displacements (Jin & Zhang, 2016), obtained by interpolating using the surface program of Generic Mapping Tool (GMT). We can estimate TWS variation using such GNSS displacement time series. The largest amplitudes of the seasonal water storage changes from GNSS displacements are found in the Rocky Mountains due to snow water and in the Mississippi River basin due to high precipitation and evapotranspiration rate there. The result is similar to GRACE time-variable gravity data and the model North American Land Data Assimilation System (NLDAS).

Severe drought monitoring with GNSS

Over 70% of the areas in the southwestern US were subject to severe drought in 2012 (Chew & Small, 2014), which are clearly observed in the vertical displacements of GNSS stations and TWS changes from GRACE gravity measurements, during the period 2012–2014 with high drought intensity (Fig. 7). The time series were obtained

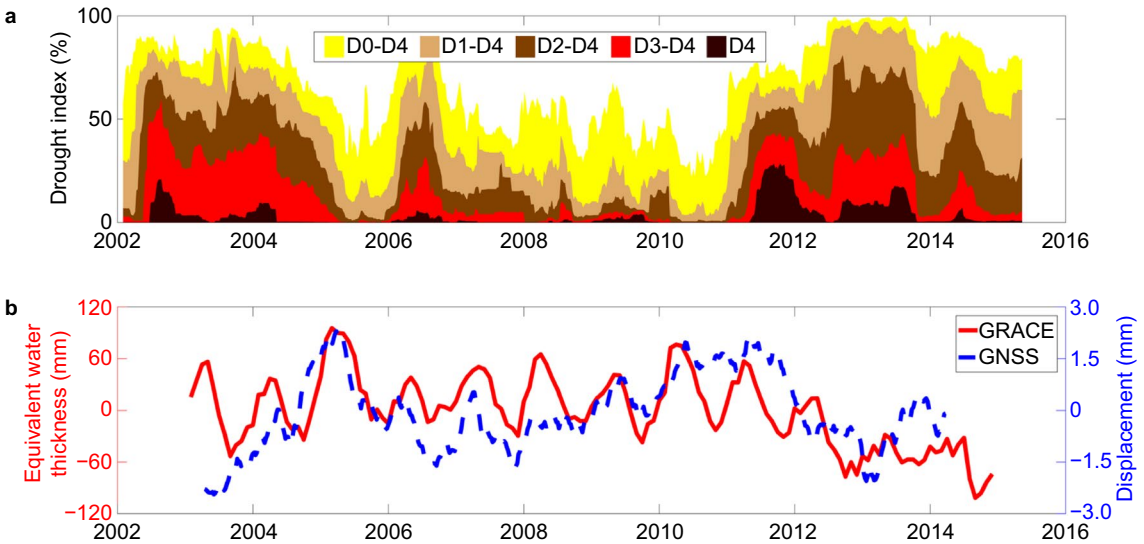

Fig. 7 **a** Drought index in southwestern US with classification D0 to D4 with increasing severity; **b** Monthly TWS anomalies from GRACE (red) and monthly TWS anomalies from GNSS vertical displacements (blue) (modified from Jin & Zhang, 2016)

from GNSS station displacements during the studied period, smoothed with a 3-month moving-average window for a better comparison with GRACE TWS change. The monthly GRACE TWS anomalies and GNSS TWS change were highly correlated with each other from 2005 to 2012. The GRACE and GNSS TWS decreased rapidly after 2012 due to severe drought and captured well the drought from 2012 to 2014 (Jin & Zhang, 2016).

Related topics

Earth's oblateness variations from GNSS data

Earth is a rotating ellipsoid, and the centrifugal force makes its dynamic oblateness referred to as J_2. Redistribution of the Earth's surface fluid, including atmosphere, ocean, and water on land, will change the oblateness with time. Currently, SLR provides the most accurate time series of J_2 (Cheng & Tapley, 2004). However, it still has large uncertainty or limitations due to the sparse and uneven distribution of SLR stations and non-continuous observations.

With the method similar to estimating surface loads using GNSS station displacements, the variation of J_2 can be estimated from the displacements of globally distributed continuously observing GNSS stations. Figure 8 compares the time series of J_2 with GNSS (300 station from International GNSS Service), GNSS + OBP (ocean bottom pressure), GNSS + OBP + GRACE, SLR, GRACE and models (Jin & Zhang, 2012).

Their annual J_2 variations show a good agreement, while GNSS alone has a smaller amplitude possibly due to the insufficient GNSS station coverage in ocean areas. The excitation of multiple timescale J_2 variations were analyzed using geophysical model data. The results show that the variations of J_2 at seasonal, intra-seasonal, and interannual timescales are mainly driven by the redistribution of Earth's surface mass including atmosphere, ocean, and land water.

Fake subsidence signals by snow accretion on antennas

Next, we discuss unrealistically large short-term subsidence signals found occasionally in snowy places during winter. Figure 9a shows time series of the up coordinates at three GNSS stations in Hokkaido, Japan, downloaded from NGL/UNR. The data with negative deviations up to 10 cm are seen from time to time in winter. Such a large subsidence and its sudden recovery is quite unlikely to occur as a response to real surface loading. These are considered as the fake signals caused by snow accretion onto the GNSS antenna radomes.

We select three short time windows when such episodes are seen, and call them Cases 1, 2, and 3. In all these cases, apparent subsidence gets large gradually and then suddenly recovers. Snow accretion is believed to start at the

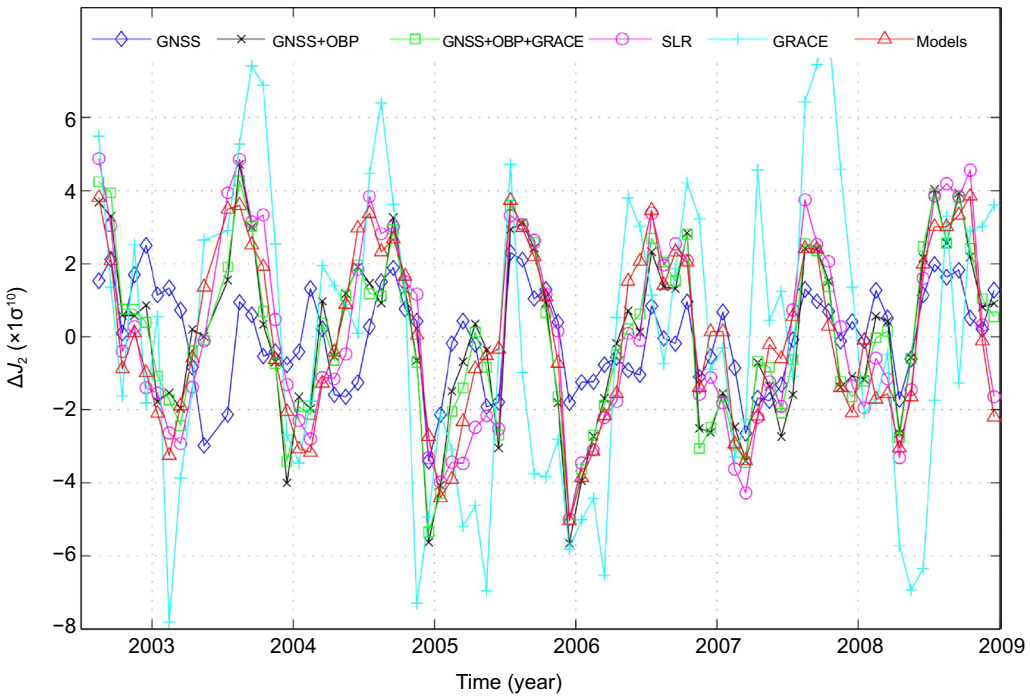

Fig. 8 Time series of the Earth's dynamic oblateness J_2 with GNSS, GNSS + OBP, GNSS + OBP + GRACE, SLR, GRACE and models (modified from Jin & Zhang, 2012)

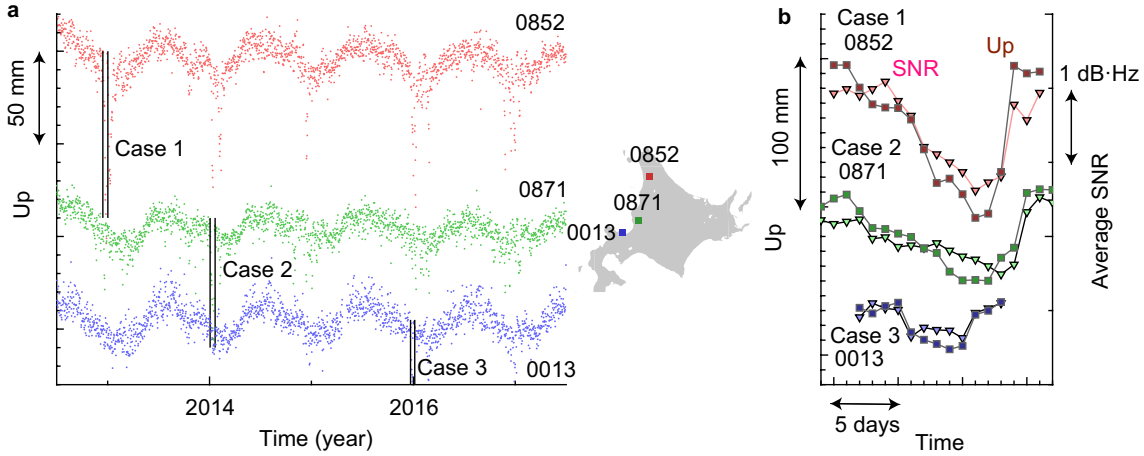

Fig. 9 GNSS stations in snowy regions often show unrealistically large subsidence. **a** Red, green, and blue dots in the time series indicate daily up positions of stations 0852, 0871, 0013 in Hokkaido, Japan (data from NGL/UNR). We select three such cases within pairs of vertical lines and magnify them in (**b**). They are artificial subsidence due to the delay of microwave signals in snow accreted to these antenna radomes, and not due to real subsidence of these stations. Such fake subsidence signals can be discriminated from real ones by plotting SNR (L2), whose decrease shows good correlations with the apparent subsidence (**b**)

time when significant snowfalls occur under relatively warm temperatures. Then, the accreted snow becomes thicker as snow continues. According to Steiner et al. (2019), the microwave velocity decreases to 1.3 (very wet snow) and 2.3 (dry snow)$\times 10^8$ m/s, when propagating through snow depending on its wetness. It is reasonable to believe that accreted snow as thick as 10–20 cm may cause apparent subsidence of 5–10 cm (azimuthal asymmetry of the accreted snow may cause apparent horizontal displacements as well). The accreted snow will eventually come off the radome and fall, which makes the coordinate suddenly recovered to the original value.

Accreted snow will not only cause phase delays but also weaken the microwave signal reaching the antenna. It then will leave some signatures in the Signal-to-Noise Ratio (SNR). Figure 9b compares time series of vertical positions and the daily average SNR of all GPS satellites with the elevations from 20 to 90 degrees. SNR decrease is clearly correlated with the apparent downward displacements suggesting that the microwave signals from satellites are partly attenuated by obstacles (snow) on the radome. Such SNR signatures are useful in discriminating real subsidence signals from fake ones due to the snow accretion.

Concluding remarks

In this paper, we briefly reviewed the history of geodetic study on surface loading. Then, we showed the examples of observed 3D seasonal crustal deformations and gravity changes, the interannual changes in seasonal movement amplitudes, and interference of two seasonally changing loads with various phase differences. We also reviewed hydrological applications of geodetic study of the crustal movements by surface loading. Finally, we showed a few related topics, change in the oblateness of the Earth as a global topic, and fake subsidence signals due to snow accretion to antenna radomes as a local topic.

We here did not introduce the study of loading using Interferometric Synthetic Aperture Radar (InSAR), but its high spatial resolution will make it an important tool in future for mapping crustal deformation by localized surface loads such as impoundment of reservoirs. Considering the variety and uniqueness of these scientific values, space geodetic study of surface loading will play important roles in geophysics in the future.

In early days, the signals of surface loading were considered as noises disturbing tectonic signals. Later, the scientific values of these signals have been recognized. Now, many people deem loading signals as valuable data. Such an "evolution", i.e., a certain quantity changes its status from a noise to a signal, emerges several times in space geodesy. For example, tropospheric delay, especially wet delay evolved from a source of noises disturbing coordinate time series to meteorological and climatological signals. Indeed, water vapor information from GEONET has been routinely used in weather forecast in Japan (e.g., Shoji, 2013).

Regarding the upper atmosphere, we used to just remove ionospheric delays by making ionosphere-free linear combinations of carrier phases in two different frequencies. Now we know they are sources of valuable information on ionospheric disturbances of various kinds (e.g., Heki, 2021; Jin et al., 2018). We anticipate such "unexpected" evolutions would repeat in the future of space geodesy.

Abbreviations

AMeDAS	Automatic meteorological data acquisition system
AO	Arctic oscillation
ENSO	El-Niño southern oscillation
GEONET	GNSS earth observation network
GMT	Generic mapping tool
GNSS	Global navigation satellite navigation
GPS	Global positioning system
GRACE	Gravity recovery and climate experiment
GSI	Geospatial Information Authority of Japan
InSAR	Interferometric synthetic aperture radar
NE	Northeast
NGL	Nevada Geodetic Laboratory
NLDAS	North American Land Data Assimilation System
OBP	Ocean bottom pressure
SLR	Satellite laser ranging
SNR	Signal-to-noise ratio
SW	Southwest
TWS	Terrestrial (total) water storage
UNR	University of Nevada, Reno
UTCSR	University of Texas, Center for Space Research
VLBI	Very long baseline interferometry
WBE	Water balance equation
3D	Three-dimensional

Acknowledgements
We thank two anonymous reviewers and Wei Feng (SYSU) for constructive comments.

Author contributions
SJ wrote 4.1, 4.2, and 5.1. KH wrote the rest. Both read and approved the final manuscript.

Funding
KH is supported by Chinese Academy of Sciences, President's International Fellowship Initiative (Grant number 2022VEA0014) and SJ is supported by the Strategic Priority Research Program Project of the Chinese Academy of Sciences (Grant No. XDA23040100).

Availability of data and materials
GNSS data used in Figs. 2 and 9 are downloaded from NGL/UNR. Those used in Figs. 3 and 5 are downloaded from GSI (terras.gsi.go.jp). GRACE mascon data in Fig. 2 are downloaded from UTCSR. UNR data are all available to researchers on the web. GSI data are available upon obtaining user IDs. Meteorological data in Japan used in Figs. 3 and 5 are downloaded from the website of the Japan Meteorological Agency (www.jma.go.jp). Figures 6, 7, and 8 are modified from those in the original articles by one of the authors.

Declarations

Competing interests
The authors declare that they have no competing interests.

Received: 21 April 2023 Accepted: 20 June 2023
Published online: 24 July 2023

References

Alothman, A. O., Bos, M., Fernandes, R., Radwan, A. M., & Rashwan, M. (2020). Annual sea level variations in the Red Sea observed using GNSS. *Geophysical Journal International, 221*, 826–834. https://doi.org/10.1093/gji/ggaa032

Argus, D. F., Fu, Y., & Landerer, F. W. (2014). Seasonal variation in total water storage in California inferred from GPS observations of vertical land motion. *Geophysical Research Letters, 41*, 1971–1980. https://doi.org/10.1002/2014GL059570

Bevis, M., Alsdorf, D., Kendrick, E., Fortes, L. P., Forsberg, B., Smalley, R., Jr., & Becker, J. (2005). Seasonal fluctuations in the mass of the Amazon River system and Earth's elastic response. *Geophysical Research Letters, 32*, L16308. https://doi.org/10.1029/2005GL023491

Blewitt, G., Hammond, W. C., & Kreemer, C. (2018). Harnessing the GPS data explosion for interdisciplinary science. *Eos, 99*, 1–2.

Bollinger, L., Perrier, F., Avouac, J.-P., Sapkota, S., Gautam, U., & Tiwari, D. R. (2007). Seasonal modulation of seismicity in the Himalaya of Nepal. *Geophysical Research Letters, 34*, L0804. https://doi.org/10.1029/2006GL029192

Cheng, M., & Tapley, B. D. (2004). Variation in the Earth's oblatenessduring the past 28 years. *Journal of Geophysical Research, 109*, B09402. https://doi.org/10.1029/2004JB003028

Chew, C. C., & Small, E. E. (2014). Terrestrial water storage response to the 2012 drought estimated from GPS vertical position anomalies. *Geophysical Research Letters, 41*, 6145–6151. https://doi.org/10.1002/2014GL061206

Davis, J. L., Elósegui, P., Mitrovica, J. X., & Tamisiea, M. E. (2004). Climate-driven deformation of the solid Earth from GRACE and GPS. *Geophysical Research Letters, 31*, L24605. https://doi.org/10.1029/2004GL021435

Dong, D., Fang, P., Bock, Y., Cheng, M. K., & Miyazaki, S. (2002). Anatomy of apparent seasonal variations from GPS-derived site position time series. *Journal of Geophysical Research, 107*, 2075. https://doi.org/10.1029/2001JB000573

Drouin, V., Heki, K., Sigmundsson, F., Hreinsdóttir, S., & Ófeigsson, B. G. (2016). Constraints on seasonal load variations and regional rigidity from continuous GPS measurements in Iceland, 1997–2014. *Geophysical Journal International, 205*, 1843–1858. https://doi.org/10.1093/gji/ggw122

Farrell, W. E. (1972). Deformation of the Earth by surface loads. *Reviews of Geophysics, 10*(3), 761–797. https://doi.org/10.1029/rg010i003p00761

Heki, K. (2001). Seasonal modulation of interseismic strain build-up in Northeastern Japan driven by snow loads. *Science, 293*, 89–92.

Heki, K. (2003). Snow load and seasonal variation of earthquake occurrence in Japan. *Earth and Planetary Science Letters, 207*, 159–164.

Heki, K. (2004). Dense GPS array as a new sensor of seasonal changes of surface loads. In R. S. J. Sparks & C. J. Hawkesworth (Eds.), *State of the planet: frontiers and challenges in geophysics*, Geophysical Monograph Ser. 150, (pp. 177–196). American Geophysical Union.

Heki, K. (2021). Chapter 21: Ionospheric disturbances related to earthquakes. In C. Huang, G. Lu, Y. Zhang, & L. J. Paxton (Eds.), *Ionospheric dynamics and applications*, Geophysics Monograph, 260 (pp. 511–526). Wiley/American Geophysical Union. https://doi.org/10.1002/9781119815617.ch21

Heki, K., & Arief, S. (2022). Crustal response to heavy rains in Southwest Japan 2017–2020. *Earth and Planetary Science Letters*. https://doi.org/10.1016/j.epsl.2021.117325

Hsu, Y. J., Kao, H., Bürgmann, R., Lee, Y. T., Huang, H. H., Hsu, Y. F., Wu, Y. M., & Zhuang, J. (2021). Synchronized and asynchronous modulation of seismicity by hydrological loading: A case study in Taiwan. *Science Advances, 7*, eabf7282. https://doi.org/10.1126/sciadv.abf7282

Jin, S. G., & Zhang, T. Y. (2016). Terrestrial water storage anomalies associated with drought in Southwestern USA derived from GPS observations. *Surveys in Geophysics, 37*(6), 1139–1156. https://doi.org/10.1007/s10712-016-9385-z

Jin, S. G., & Zhang, X. G. (2012). Variations and geophysical excitation of Earth's dynamic oblateness estimated from GPS, OBP, and GRACE. *Chinese Science Bulletin, 57*(36), 3484–3492. https://doi.org/10.1360/972011-1934

Jin, S. G., Jin, R., & Liu, X. (2018). *GNSS atmospheric seismology: Theory, observations and modeling* (p. 309). Springer.

Jin, S. G., Wang, Q., & Dardanelli, G. (2022). A review on multi-GNSS for Earth observation and emerging applications. *Remote Sensing, 14*(16), 3930. https://doi.org/10.3390/rs14163930

Johnson, C. W., Fu, Y., & Bürgmann, R. (2017). Seasonal water storage, stress modulation, and California seismicity. *Science, 356*, 1161–1164.

Lambeck, K. (2005). *The Earth's variable rotation: Geophysical causes and consequences,* Cambridge Monographs on Mechanics Series. Cambridge University Press, pp. 464, ISBN 0521673305.

Matsuo, K., & Heki, K. (2012). Anomalous precipitation signatures of the Arctic oscillation in the time-variable gravity field by GRACE. *Geophysical Journal International, 130*, 1495–1506. https://doi.org/10.1111/j.1365-246X.2012.05588.x

Milliner, C., Materna, K., Bürgmann, R., Fu, Y., Moore, A. W., Bekaert, D., Adhikari, S., & Argus, D. F. (2018). Tracking the weight of Hurricane Harvey's storm water using GPS data. *Science Advances, 4*(9), 2477. https://doi.org/10.1126/sciadv.aau2477

Morishita, Y., & Heki, K. (2008). Characteristic precipitation patterns of El Nino / La Nina in time-variable gravity fields by GRACE. *Earth and Planetary Science Letters, 272*, 677–682.
Munk, W. H., & MacDonald, G. J. F. (1960). *The rotation of the earth: A geophysical discussion* (p. 323). Cambridge University Press.
Murakami, M., & Miyazaki, S. (2001). Periodicity of strain accumulation detected by permanent GPS array: Possible relationship to seasonality of major earthquakes' occurrence. *Geophysical Research Letters, 28*, 2983–2986.
Ropelewski, C. F., & Halpert, M. S. (1996). Quantifying Southern oscillation-precipitation relationships. *Journal of Climate, 9*, 1043–1059.
Save, H. (2019). CSR GRACE RL06 mascon solutions, Texas data repository Dataverse V1, doi: https://doi.org/10.18738/T8/UN91VR.
Shoji, Y. (2013). Retrieval of water vapor inhomogeneity using the Japanese nationwide GPS array and its potential for prediction of convective precipitations. *Journal of the Meteorological Society of Japan, 91*, 43–62. https://doi.org/10.2151/jmsj.2013-103
Steiner, L., Meindl, M., & Geiger, A. (2019). Characteristics and limitations of GPS L1 observations from submerged antennas: Theoretical investigation in snow, ice, and freshwater and practical observations within a freshwater layer. *Journal of Geodesy, 93*, 267–280. https://doi.org/10.1007/s00190-018-1147-x
Takamatsu, N., Muramatsu, H., Abe, S., Hatanaka, Y., Furuya, T., Kakiage, Y., Ohashi, K., Kato, C., Ohno, K., & Kawamoto, S. (2023). New GEONET analysis strategy at GSI: Daily coordinates of over 1300 GNSS CORS in Japan throughout the last quarter century. *Earth Planets Space*. https://doi.org/10.1186/s40623-023-01787-7
Tang, H., Dong, J., Zhang, L., & Sun, W. (2020). Deformation of a spherical viscoelastic and incompressible Earth for a point load with periodic time change. *Geophysical Journal International, 222*, 1909–1922.
van Dam, T. M., & Wahr, J. M. (1987). Displacement of the earth's surface due to atmospheric loading—Effects of gravity and baseline measurements. *Journal of Geophysical Research, 92*, 1281–1286. https://doi.org/10.1029/JB0092iB02p01281
Wahr, J., Smeed, D. A., Leuliette, E., & Swenson, S. (2014). Seasonal variability of the Red Sea, from satellite gravity, radar altimetry, and in situ observations. *Journal of Geophysical Research: Oceans, 119*, 5091–5104. https://doi.org/10.1002/2014JC010161
Wang, H., Xiang, L., Jia, L., Jiang, L., Wang, Z., Hu, B., & Gao, P. (2012). Load Love numbers and Green's functions for elastic Earth models PREM, iasp91, ak135, and modified models with refined crustal structure from Crust 2.0. *Computers & Geosciences, 49*, 190–199.
Zhan, W., Heki, K., Arief, S., & Yoshida, M. (2021). Topographic amplification of crustal subsidence by the rainwater load of the 2019 typhoon Hagibis in Japan. *Journal of Geophysical Research: Solid Earth, 126*, e2021JB021845.
Zhang, L., Tang, H., & Sun, W. (2021). Comparison of GRACE and GNSS seasonal load displacements considering regional averages and discrete points. *Journal of Geophysical Research: Solid Earth, 126*(8), 1–27. https://doi.org/10.1029/2021JB021775
Zhang, X., Jin, S. G., & Lu, X. (2017). Global surface mass variations from continuous GPS observations and satellite altimetry data. *Remote Sensing, 9*(10), 1000. https://doi.org/10.3390/rs9101000
Zheng, S., Heki, K., Zhang, Z., Tokui, Y., & Yan, H. (2023). Interference of ocean and land mass changes in seasonal crustal deformation of coastal stations: A case study in norhern Australia. *Earth and Planetary Science Letters, 614*, 118212. https://doi.org/10.1016/j.epsl.2023.118212

Publisher's Note